ACS OMEGA

http://pubs.acs.org/journal/acsodf

Article

Molecularly Imprinted Polymer Modified with an MWCNT Nanocomposite for the Fabrication of a Barbital Solid-Contact Ion-Selective Electrode

Layla M. S. Al Shagri, Ayman H. Kamel,* Hisham S. M. Abd-Rabboh, and Majed A. Bajaber

Cite This: *ACS Omega* 2022, 7, 32988−32995

Read Online

ACCESS | Metrics & More | Article Recommendations

ABSTRACT: For potentiometric sensing of barbital (BAR), unique micro-sized imprinted polymer/multiwalled carbon nanotube (MWCNT)-based sensors are introduced. MWCNT is a lipophilic ion-to-electron transducing substance. A synthetic, described, and integrated barbital sodium molecular imprinted polymer (MIP) was used as a recognition receptor for potentiometric transduction in a plasticized polyvinyl chloride membrane. Methacrylic acid and ethylene glycol dimethacrylic acid are used as the functional monomer and crosslinking agent, respectively, in the synthesis of the MIPs. In the operating concentration range of 1.0×10^{-3} to 2.0×10^{-7} M, the sensors' Nernstian slope was -56.8 ± 0.9 mV/decade, with a detection limit of 1.0×10^{-7} M. The sensor displayed an accurate response time of 10 s and consistent potential response in the pH range of 8.5−11. Using chronopotentiometry tests, the interfacial capacitance of the presented ion-to-electron transducer was assessed. When compared to sensors without MWCNTs, the interfacial double-layer capacitance for sensors based on those layers reached 52.5 μF. After the addition of the MWCNTs nanocomposite layer, the water layer was eliminated between the sensing membrane and the conducting substrate. A wide range of applications for the proposed sensors for BAR detection in real samples can be provided by the sensors' strong selectivity over the interfering species. The suggested sensors were successfully used to determine BAR in urine samples that had been spiked.

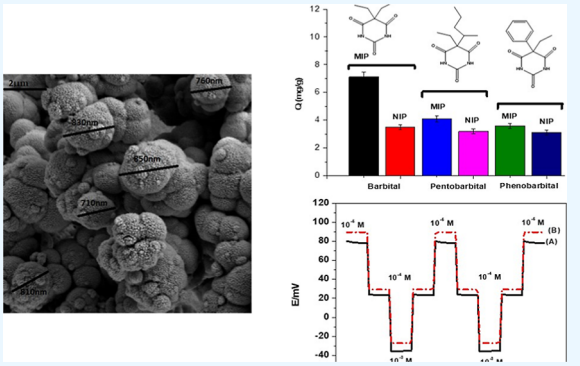

1. INTRODUCTION

Barbiturates are used in medicine to treat anxiety, hypnotize patients, and prevent seizures in addition to depressing the central nervous system.[1−3] Barbiturates have different effects depending on how much is consumed.[4−6] Barbiturates may induce relaxation and sleepiness at relatively modest doses, but at high doses, they depress the respiratory system severely. Additionally, they carry a significant danger of physical and psychological addiction that could have detrimental impacts on one's health.[5] Barbiturates have been superseded by the benzodiazepine group as sedatives/hypnotics due to their addictive qualities.[6] Currently, broad public concern has been raised about the over usage of these medications. Barbiturates monitoring is, therefore, crucial for forensic research, the creation of new formulations, and the investigation of poisoning, especially in biological material.[7]

Barbital (BAR), also known as luminal, is made from barbituric acid. Diethylmalonyl urea and diethylbarbituric acid are other names for it. In the UK, its sodium salt is marketed under the generic name Medinal. It is a long-acting barbiturate that, at large doses, inhibits most metabolic functions. BAR is primarily used to treat sleeplessness brought on by neuropathy as a sedative and hypnotic medication.[8] The human body may experience major toxic adverse effects from a BAR overdose. General weakness, nausea, headaches, respiratory depression, and mortality may result from these side effects.[9] It is also used in veterinary practice for central nervous system depression. Barbital is a schedule IV-controlled drug. The Association's hazardous effects have drawn more attention to its quantification, which is crucial for maintaining human health. The quantitative determination of BAR, which is crucial for human health, has drawn increasing attention due to the harmful effects of BAR.

Various analytical techniques, including liquid chromatography/mass spectrometry,[10] gas chromatography/mass spectrometry (GC/MS),[11] UV spectrometry,[12] liquid phase microextraction,[13] capillary electrophoresis,[14] voltammetry,[15]

Received: April 11, 2022
Accepted: August 30, 2022
Published: September 8, 2022

https://doi.org/10.1021/acsomega.2c02250
ACS Omega 2022, 7, 32988−32995

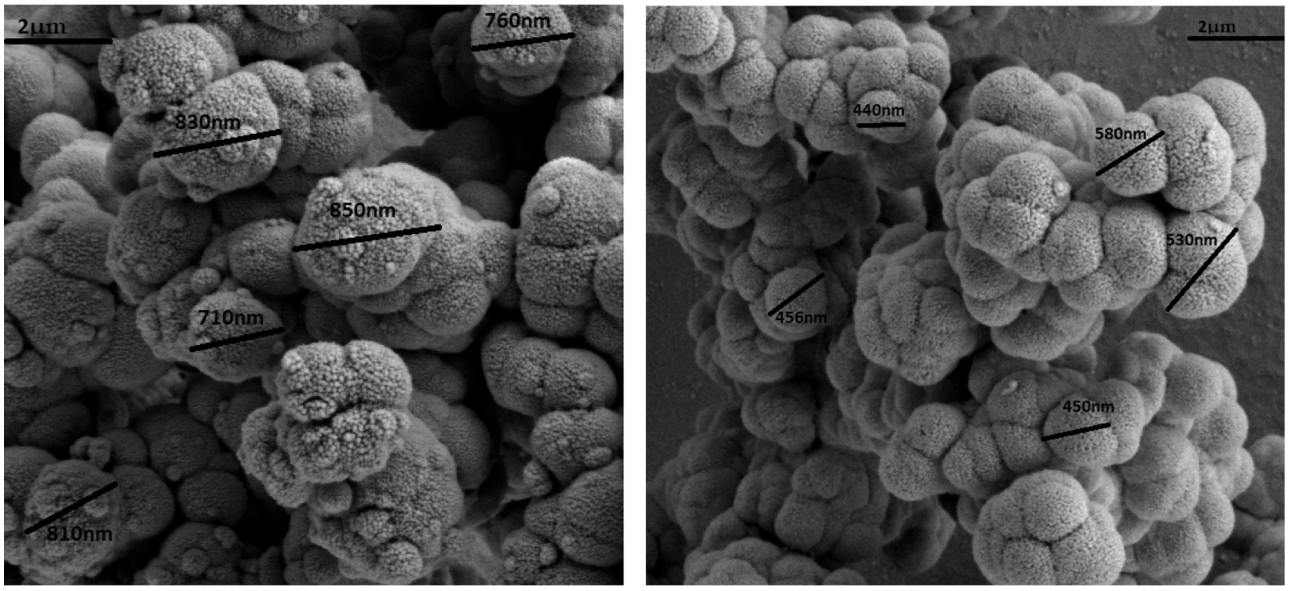

Figure 1. SEM photographs of MIPs (A) and NIPs (B) in acetonitrile solvent. [Mag. = 10.00 kx; EHT = 5.00 kV; WD = 6.9 mm].

and potentiometry,[16,17] have attracted considerable attention to BAR determination in recent decades. Traditional methods for conducting regular analyses of barbitals have been replaced by GC/MS, which has developed into an indispensable method to attain lower limits of detection.[11] However, the GC/MS analysis was regularly preceded by chemical derivatization, which is frequently time-consuming and may cause sample loss or deterioration. Additionally, the process uses pricey, bulky instruments. The use of expensive heavy equipment, sample pretreatment, laborious analytical procedures, and expensive equipment maintenance costs are still a few of the unavoidable restrictions for alternative methodologies. Therefore, it is crucial to create a quick, sensitive, and focused BAR determination procedure. Potentiometry is an electrochemical technique that has several advantages over other electrochemical techniques and can get around some of their drawbacks. It is fascinating to see how potentiometric transduction-based sensing techniques are flourishing.

Chemosensors based on molecularly imprinted polymers (MIPs) have shown rapid growth for many years.[18,19] Since the outset, the demand for straightforward instruments with the best selectivity for the detection of numerous chemicals in various fields has motivated their ongoing development. Medical diagnosis,[20] environmental and industrial monitoring,[21,22] food and toxicological analysis,[23,24] trace explosives detection, and/or the identification of their precursors are a few of these sectors.[25,26] Currently, one of the most effective techniques for developing sensitive and selective procedures is molecular imprinting. It is possible to increase the number of substances that can be detected by changing the electrode that binds the analyte. Different MIPs have been created for the selective identification of barbiturates, such as barbital, in the literature. A MIP with size-exclusion features was created and used by Haginaka et al. to extract barbiturates from river water samples.[27] The authors created their MIP using cyclobarbital as a template molecule and a readily available monomer 4-vinylpyridine (4-Vpy) as the functional monomer through a multistep swelling polymerization process. The MIP was placed in a column and connected online to a mass spectrometer-equipped chromatographic apparatus. This setup made it possible to measure the amounts of amobarbital, cyclobarbital, phenobarbital, and phenytoin in samples of river water (50 mL sample volumes). A MIP was created via precipitation polymerization using barbital as the template molecule, 2,6-bis-acrylamidopyridine as the functional monomer, and DVB-80 as the cross-linking agent, according to Beltran et al. The created MIPs were used in the solid-phase extraction (SPE) of barbiturates from human urine samples as a molecularly selective sorbent.[28] Barbital served as the template molecule and folic acid served as the functional monomer in Jing et al. electropolymerization's approach for the manufacture of a MIP. Using voltammetric methods, the MIP beads were used as a sensory component in the electrochemical detection of barbital.[15] Theoretical and experimental studies on the performances of barbital-imprinted systems were presented by Liu et al. They used density functional theory to study the interaction process between barbital and 2-vinyl-4,6-diamino-1,3,5-triazine in acetonitrile at 333 K. Barbital and 2-vinyl-4,6-diamino-1,3,5-triazine were used as the template and functional monomer, respectively. In the investigation of selective adsorption, it was discovered that MIPs had a better selectivity for barbital than for pentobarbital and 1,3-dimethyl barbituric acid.[29] Using the M062X/6-31G(d,p) density functional theory, simulations of the interaction processes between BAR and 4-Vpy were conducted (d,p).[30] The study of selective adsorption shows that BAR-MIPs have a higher selectivity for BAR than for 1,3-dimethyl barbituric acid, 2-thiobarbituric acid, and pentobarbital (PBAR).

Potentiometric sensors with MIP as a sensory component have been developed recently and exhibit promising application potential.[31,32] Due to the unique recognition sites found in MIPs, they have various advantages including low background current, a wide variety of possible windows, quick surface renewal, ease of manufacture, and improved sensitivity and selectivity. The monomer that works best for creating MIPs is methacrylic acid (MAA). This is based on changes in Gibbs free energy and interaction energies. Furthermore, by using the border molecular orbitals and molecular electrostatic potentials, the reaction sites of BAR and MAA can be

https://doi.org/10.1021/acsomega.2c02250
ACS Omega 2022, 7, 32988−32995

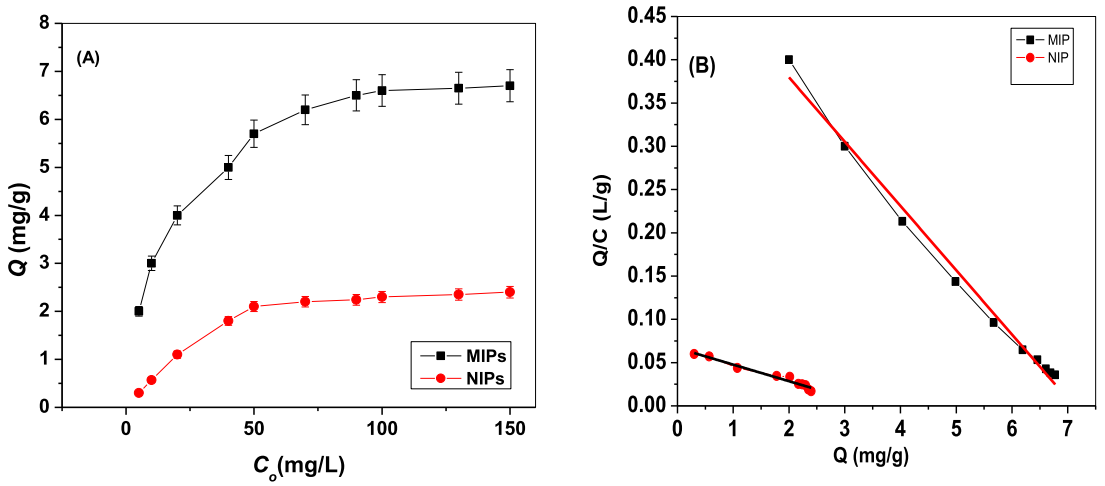

Figure 2. (A) Adsorption isotherms and (B) Scatchard plots for both MIP and NIP beads.

predicted. It can be expected that BAR can act as an electron donor, while this is based on changes in Gibbs free energy and interaction energies. Furthermore, by using the border molecular orbitals and molecular electrostatic potentials, the reaction sites of BAR and MAA can be predicted. It is reasonable to assume that BAR may function as an electron donor and MAA as an electron acceptor. MAA acts as an electron acceptor. Moreover, the BAR−MAA complex simultaneously can involve N−H···O and C═O···H double hydrogen bonds. Therefore, we can expect that MAA is suitable for BAR recognition.

Numerous nanostructured carbon materials, such as colloid-imprinted mesoporous (3DOM) carbon, carbon nanotubes, fullerene, graphene, and porous carbon spheres, have been employed as novel solid contacts.[33] Each of these materials has programmable surfaces and tightly controlled structures. These substances have a high double layer capacitance and function as solid contacts. Ion-to-electron transduction results from the electrical double layer that forms at the ISE membrane/solid contact interface.[34]

In this study, we created a novel MIP-based potentiometric sensor as a recognition component for the accurate detection of BAR. BAR and MAA serve as the template and monomer, respectively, in the synthesis of MIP. Barbital molecularly imprinted polymer (BARMIP), which is employed as a sensory component, is obtained after elution and template removal. Multiwalled carbon nanotubes (MWCNTs) were used as an ion-to-electron transducing material to modify the sensors. The sensors' sensitivity, response spectrum, selectivity, and detection limit were all characterized. Chronopotentiometric techniques were used to examine the potential stability and double-layer capacitance of the sensors that were presented. The results, which were both sensitive and selective, demonstrated that this approach may be used to identify BAR in complicated materials.

2. RESULTS AND DISCUSSIONS

2.1. Surface Morphologies of the Polymeric Particles. By precipitation free-radical polymerization with an imprinted ratio of 1:6 of BAR and MAA, respectively, the MIPs and nonimprinted polymers (NIPs) were created. Both MIP and NIP surface morphologies were characterized using scanning electron microscopy (SEM). The dimensions of the MIP and NIP particles were 810 and 580 nm, respectively, as illustrated in Figure 1. Both polymers were confirmed to be microporous by nitrogen sorption porosimetric measurement, with some mesoporosity and an average pore diameter of 29.6 A for MIP and 23.4 A for NIP, respectively. The specific surface areas were 673 ± 13 and 636 ± 17 m^2/g in the same order as earlier, while the pore volumes were 0.31 and 0.28 cm^3/g for the MIP and the NIP, respectively. Larger particle diameters, average pore diameters, pore volumes, and specific regions were discovered by MIPs. This is explained by the structure of the imprinted molecules (BAR) in the MIPs, which take up a specific amount of room within the polymer's skeleton.

2.2. Adsorption Isotherm and Scatchard Plot. As the initial concentration of BAR rises, more BAR is absorbed by MIP particles, as seen in Figure 2A. For MIP and NIP particles, the plateau, which is corresponding to the saturated adsorption capacity, reaches 7.2 and 2.7 mg/g, respectively. This proves that MIPs had a better specific adsorption capacity than NIPs did for nonspecific adsorption. This is explained by the fact that template molecules exist and participate in the production of MIPs. As a result, the MIPs now have active cavities that are compatible with the template BAR and possess active functional groups that perform a complementary role in strongly identifying the template molecules. Because NIP particles lack these specialized cavities with the spatial structure and functional groups that will match the template molecules, as can be observed in Figure 2, they have a lower adsorption capacity.

Scatchard analysis was also carried out to evaluate the maximum binding capacity Q_{max} using a Scatchard plot constructed by eq 1

$$Q/C = (Q_{max} - Q)/K_d \quad (1)$$

where Q_{max} (mg/g) is the apparent maximum adsorption capacity, K_d (mg/L) is the dissociation constant, C (mg/L) is the starting concentration of BAR, and Q (mg/g) is the number of MIPs that bind to BAR. The results are depicted in Figure 2B and demonstrate that the Scatchard model has a Q/C value of 0.5281−0.0742Q and that the adsorption isotherms of MIPs toward the BAR are in good agreement with linearity. According to the equation, MIPs have equal class binding sites for BAR within the investigated concentration range, and their respective K_d and Q_{max} values for MIPs and NIPs were 13.47 mg/L and 7.11 ± 0.4 mg/g and 52.25 mg/L and 3.49 mg/g.

https://doi.org/10.1021/acsomega.2c02250
ACS Omega 2022, 7, 32988−32995

These findings demonstrated that the binding association constants of MIPs are higher than those of NIPs.

2.3. Study of Adsorption Selectivity. For BAR, pentobarbital (PBAR), and phenobarbital (PHBAR), the selectivity of MIP and NIP particles was examined. According to Figure 3, it was discovered that MIPs had a higher ability for adsorption toward BAR than PBAR and PHBAR. This is so that the shape, size, and active sites of MIPs' imprinted cavities could not exactly match those of PBAR and PHBAR. Additionally, the NIPs are not specialized binding characteristics, making them a generic adsorbent to BAR, PBAR, and PHBAR.

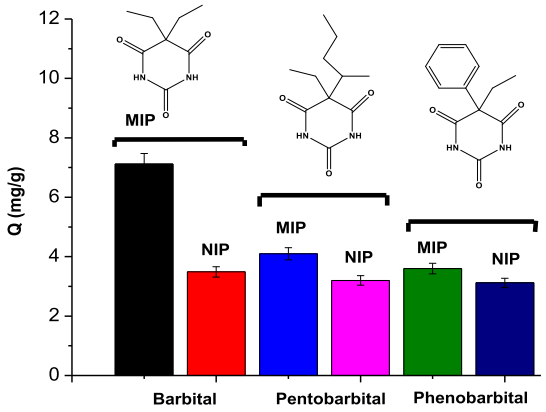

Figure 3. Adsorption selectivity of MIPs and NIPs to BAR, PBAR, and PHBAR.

2.4. Potentiometric Characteristics. *2.4.1. Potentiometric Barbital Response.* Herein, the potentiometric response based on MIPs (GC/MWCNTs/MIP/BAR-ISE) toward barbital anion was revealed by the presented sensors. The potential response was recorded in different BAR concentrations varying from 10^{-8} to 10^{-3} M to evaluate the sensitivity in terms of slope (mV/decade), the detection limit, and the linear range. As shown in Figure 4, MIP-based sensors demonstrated a Nernstian slope of −56.8 ± 0.9 mV/decade (R^2 = 0.998) across a linear range of 1.0×10^{-3} to 2.0×10^{-7} M. This linear range covers the monitoring relevant range of BAR in various samples. The limit of detection was determined at 1.0×10^{-7} M. The response of the presented sensors was rapid and reaches a stable potential at a time <5 s (the inset, Figure 4).

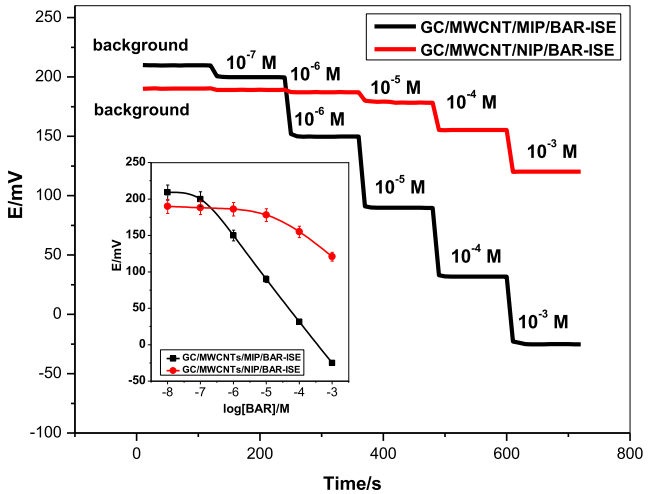

Figure 4. Calibration plots for both MIP and NIP membrane-based sensors.

As a control, membrane sensors based on NIP nanobeads (GC/MWCNTs/NIP/BAR-ISE) were also tested for BAR detection. A worse response performance was observed toward BAR than the response obtained by GC/MWCNTs/MIP/BAR-ISE for all measuring concentrations under the same conditions (Figure 4). The sensors exhibited anionic slopes of −28.5 ± 3.3 (r^2 = 0.996) mV/decade over the linear range of 1.0×10^{-3} to 6.0×10^{-5} M and the detection limit of 1.5×10^{-5} M. It was noted that the response time for GC/MWCNTs/NIP/BAR-ISE electrodes is less than 10 s. The analytical features and the potentiometric response of the proposed sensors in the presence and absence of MWCNTs layers are presented in Table 1.

2.4.2. Effect of pH on the Potentiometric Response. Utilizing two BAR concentrations, the potential stability of the provided sensors throughout a range of pH values was tested (1.0×10^{-4} and 1.0×10^{-3} M). A 0.1 M HCl/NaOH solution was used to alter the pH value. Over the pH range of 8.5−11, the sensors demonstrated a consistent potential response. This shows that the sensors can detect BAR in its anionic state. Due to the development of the nonsensed neutral barbital (pK_a = 8.14), a potential drift was seen below pH 8.0.[35] Therefore, 30 mM HCO_3^-/CO_3^{2-} buffer at pH 10.0 was used for all measurements.

2.4.3. Long-term Potential Stability. Long-term potential stability of the presented electrodes in the presence and absence MWCNTs was evaluated via systematic calibration (e.g., twice a week) and estimating the E^0 value each time from the linear segment of the calibration curve (e.g., $\Delta E^0/\Delta t$). The stability was calculated from the difference of E^0 values obtained in the last and the first calibration and then divided by the number of days between them. For three months, the calibration plots obtained showed repeatable results. As shown in Figure 5, GC/MWCNTs/MIP/BAR-ISE sensors revealed higher potential stability (e.g., $\Delta E^0/\Delta t$ = 0.28 mV/day) than GC/MIP/BAR-ISE ($\Delta E^0/\Delta t$ = 0.65 mV/day). All MWCNT-based sensors exhibited improved long-term potential stability compared to simple coated disc electrodes.

2.4.4. Short-term Stability of the Potential. Short-term potential stability was evaluated using Bobacka's method.[36] The measurements were carried out for both the modified (GC/MWCNTs/MIP/BAR-ISE) and nonmodified (GC/MIPs/BAR-ISE) electrodes in a 1.0×10^{-3} M BAR solution. The modified sensor showed better potential stability compared to the unmodified one. The determined potential drift ($\Delta E/\Delta t$) was found to be 2.11 μV/s and a high double-layer capacitance of 473.9 μF for GC/MWCNTs/MIP/BAR-ISE. For GC/MIPs/BAR-ISE sensors, they suffered from a high potential drift of 28.67 μV/s and low capacitance of 34.87 μF.

2.4.5. Reversibility of the Electrode Potential. The potential reversibility of the proposed sensors was measured in different BAR concentrations (e.g., 10^{-5}, 10^{-4}, and 10^{-3} M). Time-dependent potential traces during reversibility measurements were presented in Figure 6. The mean potential values obtained from measurements in particular concentrations were 89.2 ± 1.6, 29.6 ± 1.6, and −27.0 ± 1.9 mV for the concentrations 10^{-5}, 10^{-4}, and 10^{-3} M, respectively. For the nonmodified GC/MIPs/BAR-ISE electrodes, the mean

https://doi.org/10.1021/acsomega.2c02250
ACS Omega 2022, 7, 32988−32995

Table 1. Analytical Features and the Potentiometric Response of the Proposed Sensors

parameters	GC/MIP/BAR-ISE	GC/MWCNTs/MIP/BAR-ISE	GC/NIP/BAR-ISE	GC/MWCNTs/NIP/BAR-ISE
slope (mv/decade)	53.4 ± 1.2	−56.8 ± 0.9	25.2 ± 1.3	−28.5 ± 3.3
detection limit, (M)	7.0×10^{-7}	1.0×10^{-7}	1.5×10^{-5}	1.5×10^{-5}
correlation coefficient (r^2)	0.997	0.998	0.997	0.996
linear range, (M)	1.0×10^{-6} to 1.0×10^{-3}	1.0×10^{-3} to 2.0×10^{-7}	6.0×10^{-5} to 1.0×10^{-3}	1.0×10^{-3} to 6.0×10^{-5}
response time, (s)	<5	<5	<10	<10
pH range	8.5−11	8.5−11	8.5−11	8.5−11
precision, (%)	0.9	1.1	1.6	1.2
accuracy, (%)	99.2	99.5	98.7	98.5
standard deviation, (mV)	±1.4	±0.9	±1.2	±1.6

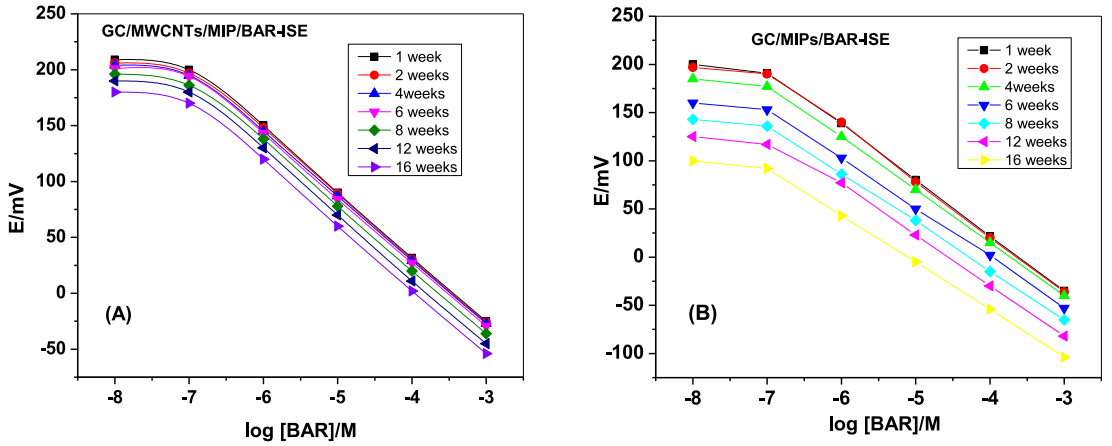

Figure 5. Calibration curves of the presented sensors (A) with and (B) without the MWCNT intermediate layer, determined in time.

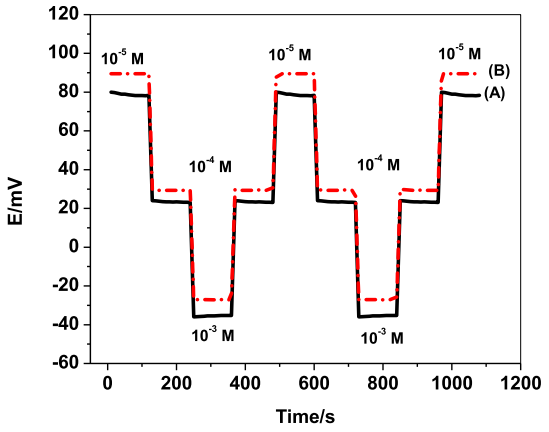

Figure 6. Reversibility of the potential response measured in BAR solutions with concentrations: 1.0×10^{-5}, 1.0×10^{-4}, and 1.0×10^{-3} M for the presented sensors: (A) GC/MIPs/BAR-ISE and (B) GC/MWCNTs/MIP/BAR-ISE.

potential values obtained from measurements in particular concentrations were 79.6 ± 2.6, 23.6 ± 0.6, and −35.6 ± 1.4 mV for the concentrations 10^{-5}, 10^{-4}, and 10^{-3} M, respectively. Sensors modified with MWCNTs were characterized by better potential reversibility than nonmodified electrode ISE.

2.5. Selectivity. Selectivity coefficients ($K_{BAR,J}^{pot}$) for some selected interfering ions were evaluated using the modified separate solution method suggested by Bakker.[37] The log $K_{BAR,J}^{pot}$ values were shown in Table 2. Insertion of an intermediate layer of MWCNTs between the electronic conductor in the electrode and the ion-sensing membrane did not change the selectivity significantly. Different barbital analogues such as phenobarbital and pentobarbital were chosen for testing their interfering effect. The electrodes based on MIPs showed enhanced selectivity toward BAR over the abovementioned ions. The obtained data proved the successful imprinting process and the high affinity of these MIPs toward an enhanced recognition of BAR template molecules.

2.6. Water-layer Test. A water-layer test was conducted to verify whether a thin layer of the water phase was formed between the electronic-conducting substrate and the ion-sensitive membrane, which could cause deterioration in the potential stability of the electrode. It was performed for both GC/MWCNTs/MIPs/BAR-ISE and GC/MIPs/BAR-ISE electrodes after soaking in 1.0×10^{-3} M BAR solution

Table 2. Selectivity Coefficients for GC/MWCNTs/MIPs/BAR-ISE and GC/MIPs/BAR-ISE

	log $K_{BAR,J}^{pot}$ ± SD[a]					
sensor	pentobarbital	phenobarbital	valsartan	oxalate	Cl^-	NO_3^-
GC/MWCNTs/MIPs/BAR-ISE	−2.5 ± 0.2	−2.7 ± 0.3	−4.1 ± 0.1	−4.5 ± 0.3	−5.1 ± 0.3	−4.7 ± 0.5
GC/MIPs/BAR-ISE	−2.45 ± 0.3	−2.6 ± 0.1	−4.2 ± 0.2	−4.6 ± 0.1	−5.0 ± 0.2	−4.6 ± 0.3

[a]SD standard deviation (n = 3).

https://doi.org/10.1021/acsomega.2c02250
ACS Omega 2022, 7, 32988−32995

overnight. Then the potential signal was measured for about an hour in the main BAR solution, then the solution was changed to 1.0×10^{-2} M NaCl (interfering ion) and the signal was measured for about 3 h. After, the electrodes were inserted back into the main BAR solution. The change in electrode potentials was measured again for 20 h. As shown in Figure 7,

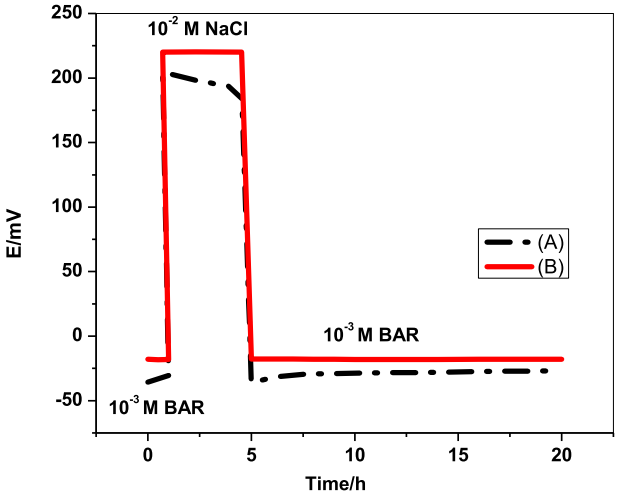

Figure 7. Water-layer test for the presented sensors: (A) GC/MIPs/BAR-ISE and (B) GC/MWCNTs/MIP/BAR-ISE. The measurements were recorded in 1.0×10^{-3} M BAR and 1.0×10^{-2} M NaCl.

GC/MIPs/BAR-ISE electrodes exhibited an observed potential drift after the replacement of BAR ions by NaCl. This indicates the formation of a water layer between the ion-sensing membrane and the electronic conductor. For sensors based on MWCNTs (e.g., GC/MWCNTs/MIPs), a less potential drift was noticed. This confirms the high lipophilicity of the MWCNTs layer and its successful role in obtaining high potential stability for the proposed sensors.

2.7. Effect of Light, O_2, N_2, and CO_2. Studying the effects of several gases, including CO_2, O_2, and N_2, and light on the potential stability allowed researchers to test the robustness of the SPE/MWCNTs/MIP-ISE. The test involved bubbling the gases for 30 min while monitoring the sensor's potential response in a 10 mM BAR solution. After submerging the MWCNT-based electrode in a 10 mM PHO solution with or without ambient light, the effect of light was assessed. No potential drifts were noticed while these effects were present, as shown in Figure 8. This shows that the provided electrode is effectively resistant to CO_2, O_2, N_2, and light interference.

2.8. Water Contact Angle Measurements. To create a coherent layer, MWCNTs were drop-cast on a glass plate after being suspended in tetrahydrofuran (THF) (5 mg/mL). Using a Dyno-Lite USB digital microscope, we captured photos of 2 L water droplets on the surfaces under study and processed the images in Inkscape 0.92.3 to estimate the water contact angles. A hydrophobic surface with water contact angles of 95° was given by the MWCNTs, which appears to support the creation of solid-contact, ion-selective electrodes.

2.9. Recovery Measurements of BAR in Spiked Urine Sample. Barbital monitoring is important because it could aid in the quick identification of an overdosed patient in a biological liquid as complicated as human urine. As a result, after diluting the human urine sample with HCO_3^-/CO_3^{2-} buffer (30 mM, pH 10.0), we added various concentrations of BAR in a ratio of 1:5. The sensors were used to perform the

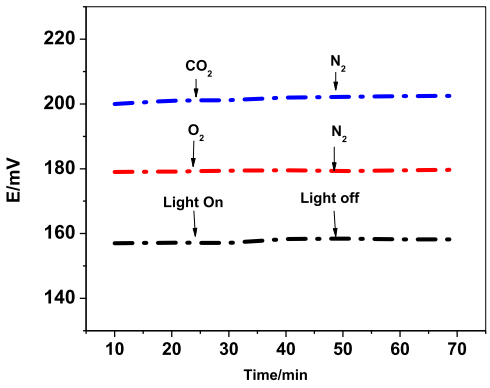

Figure 8. Effect of light, O_2, N_2, and CO_2 on the SPE/MWCNTs/MIP-ISE.

potentiometric measurements. As shown in Table 3, despite the presence of different species in the human urine sample

Table 3. Recovery Values for BAR Determination in Spiked Urine Samples

sample no.	spiked, μM	found, μM[a]	recovery, 100%	RSD, %
1	2.0	1.93 ± 0.1	96.5	0.70
2	5.0	4.87 ± 0.09	97.4	0.50
3	10.0	10.14 ± 0.58	101.4	0.30

[a]Average of 3 measurements (n = 3).

(such as Na^+, K^+, Mg^{2+}, Ca^{2+}, and urea), the provided sensors demonstrated remarkable BAR recovery. The fact that these species did not interfere with the observations demonstrates the robustness, selectivity, and application of the suggested sensors.

3. CONCLUSIONS

In this study, MWCNTs were employed to modify all-solid-state screen-printed platforms for the sensitive and specific detection of BAR. The analytical tool is dependable, affordable, and incredibly sensitive and selective. As an identification component, the polyvinyl chloride (PVC)-membrane sensors were built using uniform MIP beads. MAA and ethylene glycol dimethacrylate (EGDMA) are used as the crosslinking agent and functional monomer, respectively, in the synthesis of the MIPs. The effectiveness of the MWCNT ion-to-electro transducer layers in enhancing the potential stability and removing the water layer was proven by evaluations of the proposed sensors' long- and short-term potential stability in the presence and absence of these layers. The sensors exhibited a detection limit of 1.0×10^{-7} M with a sensitivity slope of -56.8 ± 0.9 mV/decade over the working concentration range of 1.0×10^{-3} to 2.0×10^{-7} M. The sensors were able to achieve high selectivity across a range of species, making them usable in samples with complicated compositions. In summary, the suggested potentiometric method has many advantages over many earlier methods, which can need complicated processing steps or have numerous drawbacks.

4. EXPERIMENTAL SECTION

4.1. Apparatus. Using a field-emission scanning electron microscope [German-made ZEISS Sigma 300VP electron microscope system], all polymeric beads were described and examined. Using a pH/mV meter (PXSJ-216 INESA, Scientific

https://doi.org/10.1021/acsomega.2c02250
ACS Omega 2022, 7, 32988−32995

Instrument Co., Ltd., Shanghai, China), all potentiometric measurements were performed at 25 ± 1 °C. Metrohm's galvanostat and potentiostat were used to conduct chronopotentiometry (CP) measurements (Autolab, model 204, NOVA 1.1 software: Metrohm Autolab B.V. Utrecht, The Netherlands). A three-electrode cell was used, consisting of a working electrode that is barbiton-selective (GC/MWCNTs/MIP/BAR-ISE) and an auxiliary electrode that is a Pt wire filled with 10 percent (w/v) KNO3 and an Ag/AgCl double-junction reference electrode (6.0729.100, Metrohm AG CH-9101 HERISAU, Switzerland). After providing a constant current of 1 nA to the working barbiton electrode for 60 s, followed by a reversed current for an additional 60 s, all chronopotentiometry tests were completed.

4.2. Chemicals and Reagents. The following chemicals were purchased from Sigma-Aldrich: MAA, MWCNTs, barbiton sodium salt, methanol, acetonitrile, high molecular weight PVC, *o*-nitrophenyl octyl ether (*o*-NPOE), PBAR, PHBAR, tridodecylmethylammonium chloride (TDMAC), EGDMA, and tetradodecylammonium tetrakis(4-chlorophenyl)borate (ETH 500). THF and benzoyl peroxide (BPO) were bought from Fluka. The use of all other reagents, which were of analytical quality, was without additional purification. Freshly deionized water (18.2 M cm specific resistance) was used to make all aqueous solutions using the Milli-Q PLUS reagent-grade water system (Millipore, Burlington, MA, USA).

4.3. Synthesis of MIPs. Synthesis of MIPs was carried out by mixing 0.5 mmol of the template BA with 3.0 mmol of the monomer MAA for 1 h. 3.0 mmol of the cross-linker EGDMA with 70 mg of the free-radical initiator BPO was then added and dissolved in 20 mL of acetonitrile in a glass-capped bottle. The mixture was then subjected to sonication for 5 min till the solution became homogeneous. The solution mixture was purged for 10 min with a flow of N_2 to expel all dissolved oxygen. During the 18 h polymerization procedure, an oil bath at 80 °C was used. The template was eliminated by batch-mode solvent extraction using methanol/acetic acid (8/2, v/v) and methanol once the polymer had formed. The resulting polymer was allowed to dry for an entire night at 40 °C. As previously noted, the NIPs beads were also created, but without the template molecule.

4.4. Adsorption Experiments. A 50 mL closed Erlenmeyer container containing 10 mL of BAR solution with a concentration of [5.0−150.0 g/mL] was filled with 20 mg of MIP to evaluate the MIP adsorption capability of BAR. For 6 h, the mixture was mixed at room temperature. Through a membrane filter with a 0.22 m pore size, the MIP was isolated. Using UV visible absorption spectra at a maximum wavelength of 208 nm, the remaining BAR content was calculated. Three separate binding procedures were used to calculate the balance's absorption capability. Following the application of eq 2, the equilibrium adsorption quantity (Q, mmol/g) was determined, and the related adsorption isotherms and kinetics curves were created.

$$Q = (C_0 - C)V/m \quad (2)$$

where the initial and equilibrium concentrations of BAR, respectively, are C_0 (mg/L) and C (mg/L). The total volume of the solution is V (mL), and the weight of the BAR-MIPs or NIPs is m (mg).

4.5. Preparation of GC/MWCNTs/MIP/BA-ISE. The glassy carbon electrode (GCE) was polished using 0.05 mm—Al_2O_3 slurries and then rinsed with deionized water. The GC diameter of the GCE was 3 mm. For thorough cleaning, the electrodes were sonicated in acetone for 10 min. 10 mg of MWCNTs were dissolved in 2 mL of THF and sonicated for 2 h. The resulting mixture was drop-cast in a volume of 50 L onto the polished GCE surface above. Using an IR lamp, the solution was dried for 30 s. To create the MIP-membrane-based sensor, 30 mg of any MIP beads were combined with 2.1 mg TDMAC, 3.43 mg ETH 500, 32.3 mg PVC, and 62.17 mg *o*-NPOE. They were all dissolved in 3 mL of THF. For comparison, blank NIP membranes were created using the same method but with NIPs in place of the MIP beads. By drop-casting addition, 100 L of the membrane cocktail was put above the transducing layer and left to dry for 6 h. All the electrodes were placed in a buffer of 30 mM carbonate solution, pH 10, to condition them.

AUTHOR INFORMATION

Corresponding Author

Ayman H. Kamel − *Chemistry Department, College of Science, University of Bahrain, Sakhir 32038, Kingdom of Bahrain; Department of Chemistry, Faculty of Science, Ain Shams University, Cairo 11566, Egypt;* orcid.org/0000-0001-7502-6668; Email: ahkamel76@sci.asu.edu.eg, ahmohamed@uob.edu.bh

Authors

Layla M. S. Al Shagri − *Chemistry Department, College of Science, University of Bahrain, Sakhir 32038, Kingdom of Bahrain*

Hisham S. M. Abd-Rabboh − *Chemistry Department, Faculty of Science, King Khalid University, Abha 61413, Saudi Arabia*

Majed A. Bajaber − *Chemistry Department, Faculty of Science, King Khalid University, Abha 61413, Saudi Arabia*

Complete contact information is available at: https://pubs.acs.org/10.1021/acsomega.2c02250

Author Contributions

H.S.M.A.-R. and A.H.K. provided the concepts of the work and interpreted the results; A. H. K. and L.A.M.S.A performed the experimental part and prepared the manuscript; A.H.K., H.S.M.A.-R., and L. M. S. A. cooperated in the preparation of the manuscript; A.H.K. performed the revision before submission; M. A. B. obtained financial support for the work. All authors have read and agreed to the published version of the manuscript.

Funding

This research was funded by the Deanship of Scientific Research at King Khalid University through the Research Group Program under grant number RGP.2/183/43.

Notes

The authors declare no competing financial interest.

REFERENCES

(1) Swarbrick, J. *Encyclopedia of Pharmaceutical Technology*, 3rd ed.; CRC Press: Boca Raton, FL, USA, 2013.

(2) Yasiry, Z.; Shorvon, S. D. How phenobarbital revolutionized epilepsy therapy: The story of phenobarbital therapy in epilepsy in the last 100 years. *Epilepsia* **2012**, *53*, 26−39.

(3) López-Muñoz, F.; Ucha-Udabe, R.; Alamo, C. The history of barbiturates a century after their clinical introduction. *Neuropsychiatr. Dis. Treat.* **2005**, *1*, 329.

(4) Ito, T.; Suzuki, T.; Wellman, S. E.; Ho, K. Pharmacology of barbiturate tolerance/dependence: GABAA receptors and molecular aspects. *Life Sci.* **1996**, *59*, 169−195.
(5) Vlasses, P. H.; Rocci, M. L.; Koffer, H.; Ferguson, R. K. Combined phenytoin and phenobarbital overdose. *Drug Intell. Clin. Pharm.* **1982**, *16*, 487−488.
(6) Fritch, D.; Blum, K.; Nonnemacher, S.; Kardos, K.; Buchhalter, A. R.; Cone, E. J. Barbiturate detection in oral fluid, plasma, and urine. *Ther. Drug Monit.* **2011**, *33*, 72−79.
(7) Coupey, S. M. Barbiturates. *Pediatr. Rev.* **1997**, *18*, 260−265.
(8) Ward, J. M.; Hagiwara, A.; Anderson, L. M.; Lindsey, K.; Diwan, B. A. The chronic hepatic or renal toxicity of di(2-ethylhexyl) phthalate, acetaminophen, sodium barbital, and phenobarbital in male B6C3F1 mice: Autoradiographic, immunohistochemical, and biochemical evidence for levels of DNA synthesis not associated with carcinogenesis or tumor promotion. *Toxicol. Appl. Pharmacol.* **1988**, *96*, 494−506.
(9) Fujimori, H. M. D. Potentiation of barbital hypnosis as an evaluation method for central nervous system depressants. *Psychopharmacologia* **1965**, *7*, 374−378.
(10) Zhang, F.; Ding, F.; Chu, X. G.; et al. Simultaneous determination of three barbitals in feeds by ultra-performance liquid chromatography- quadrupole-time-of-flight mass spectrometry. *Chin. J. Anal. Chem.* **2011**, *39*, 788−792.
(11) Zhao, H. X.; Qiu, Y. M.; Wang, L. P. Simultaneous determination of three barbiturates in pork by gas chromatography-mass-spectrometry. *Chin. J. Anal. Chem.* **2005**, *33*, 777−780.
(12) Abbaspour, A.; Mirzajani, R. Simultaneous determination of phenytoin, barbital and caffeine in pharmaceuticals by absorption (zero-order) UV spectra and first-order derivative spectra-multivariate calibration methods. *J. Pharm. Biomed. Anal.* **2005**, *38*, 420−427.
(13) Huang, X.; Ma, G. H.; Wang, F. L. Determination of aminopyrine, antipyrine and barbital in urine using liquid phase microextraction-gas chromatography. *Chin. J. Anal. Lab.* **2008**, *27*, 66−68.
(14) Yue, M. E.; Xu, J.; Hou, W. G. Direct determination of barbiturates in urine by capillary zone electrophoresis using β-cyclodextrin and α-cyclodextrin as additive. *Chem. Reagents* **2010**, *32*, 623−625.
(15) Zheng, J.; Yan, Z.; Mandong, G. Preparation and Application of Electrochemical Barbital Sensor Based on Molecularly Imprinting Technique. *Wuhan Univ. J. Nat. Sci.* **2017**, *22*, 207−214.
(16) Lin, W. R.; Zhang, H. X. Determination of barbitals by potentiometric double-piont-titration. *Chem. Reagents* **1993**, *12*, 50−52.
(17) Lima, J. L. F. C.; Montenegro, M. C. B. S. M.; Alonso, J.; Bartroli, J.; Raurich, J. G. 5,5-Diethylbarbiturate tubular electrode for use in flow-injection detection systems. *Anal. Chim. Acta* **1990**, *234*, 221−225.
(18) Leibl, N.; Haupt, K.; Gonzato, C.; Duma, L. Molecularly Imprinted Polymers for Chemical Sensing: A Tutorial Review. *Chemosensors* **2021**, *9*, 123−141.
(19) Adumitrăchioaie, A.; Terti, M.; Cernat, A.; Săndulescu, R.; Cristea, C. Electrochemical Methods Based on Molecularly Imprinted Polymers for Drug Detection. A Review. *Int. J. Electrochem. Sci.* **2018**, *13*, 2556−2576.
(20) Kamel, A. H.; Amr, A. E.-G.; Ashmawy, N. H.; Galal, H. R.; Al-Omar, M. A.; Sayed, A. Y. A. Solid-Contact Potentiometric Sensors Based on Stimulus-Responsive Imprinted Polymers for Reversible Detection of Neutral Dopamine. *Polymers* **2020**, *12*, 1406.
(21) Moreira, F. T. C. M.; Guerreiro, J. R. L.; Azevedo, V. L.; Kamel, A. H.; Sales, M. G. F. New biomimetic sensors for the determination of tetracycline in biological samples: Batch and flow mode operations. *Anal. Methods* **2010**, *2*, 2039−2045.
(22) Abd-Rabboh, H. S. M.; Kamel, A. H. Mimicking a receptor for cyanide ion based on ion imprinting and its applications in potential transduction. *Electroanalysis* **2012**, *24*, 1409−1415.
(23) Kamel, A. H.; Soror, T. Y.; Al Romian, F. M. Flow through potentiometric sensors based on molecularly imprinted polymers for selective monitoring of mepiquat residue, a quaternary ammonium herbicide. *Anal. Methods* **2012**, *4*, 3007−3012.
(24) Kamel, A. H.; Sayour, H. E. M. Flow-Through Assay of Quinine Using Solid Contact Potentiometric Sensors Based on Molecularly Imprinted Polymers. *Electroanalysis* **2009**, *21*, 2701−2708.
(25) Lu, W.; Min, X.; Zhibin, X.; Xiao, D.; Fei, X.; Fengyan, W.; Qiuhong, W.; Zihui, M. Molecularly Imprinted Polymers for the Sensing of Explosives and Chemical Warfare Agents. *Curr. Org. Chem.* **2015**, *19*, 62−71.
(26) Yilmaz, E.; Garipcan, B.; Patra, H. K.; Uzun, L. Molecular Imprinting Applications in Forensic Science. *Sensors* **2017**, *17*, 691.
(27) Hoshina, K.; Horiyama, S.; Matsunaga, H.; Haginaka, J. Molecularly imprinted polymers for simultaneous determination of antiepileptics in river water samples by liquid chromatography-tandem mass spectrometry. *J. Chromatogr. A* **2009**, *1216*, 4957.
(28) Beltran, A.; Borrull, F.; Cormack, P. A. G.; Marcé, R. M. Molecularly imprinted polymer with high-fidelity binding sites for the selective extraction of barbiturates from human urine. *J. Chromatogr. A* **2011**, *1218*, 4612−4618.
(29) Liu, J.; Wang, Y.; Su, T.; Li, B.; Tang, S.; Jin, R. Theoretical and experimental studies on the performances of barbital-imprinted systems. *J. Sep. Sci.* **2015**, *38*, 4105−4110.
(30) Tingting, S.; Junbo, L.; Shanshan, T.; Ruifa, J. Design and properties of barbital imprinting system with 4-vinylpyridine as functional monomer. *Gaofenzi Cailiao Kexue Yu Gongcheng* **2015**, *31*, 5−10.
(31) Alberti, G.; Zanoni, C.; Losi, V.; Magnaghi, L. R.; Biesuz, R. Current Trends in Polymer Based Sensors. *Chemosensors* **2021**, *9*, 108.
(32) Elugoke, S. E.; Adekunle, A. S.; Omolola, E.; Fayemi, O. E.; Akpan, E. D.; Mamba, B. B.; Sherif, E. M.; Ebenso, E. E. Molecularly imprinted polymers (MIPs) based electrochemical sensors for the determination of catecholamine neurotransmitters − Review. *Electrochem. Sci. Adv.* **2021**, *1*, 202000026.
(33) Hu, J.; Stein, A.; Bühlmann, P. Rational design of all-solid-state ion-selective electrodes and reference electrodes. *Trends Anal. Chem.* **2016**, *76*, 102−114.
(34) Crespo, G. A.; Macho, S.; Rius, F. X. Ion-selective electrodes using carbon nanotubes as ion-to-electron transducers. *Anal. Chem.* **2008**, *80*, 1316−1322.
(35) Compound Barbital. https://pubchem.ncbi.nlm.nih.gov.
(36) Bobacka, J. Potential Stability of All-Solid-State Ion-Selective Electrodes Using Conducting Polymers as Ion-to-Electron Transducers. *Anal. Chem.* **1999**, *71*, 4932−4937.
(37) Bakker, E. Determination of Unbiased Selectivity Coefficients of Neutral Carrier-Based Cation-Selective Electrodes. *Anal. Chem.* **1997**, *69*, 1061−1069.

https://doi.org/10.1021/acsomega.2c02250
ACS Omega 2022, 7, 32988−32995